THE JOURNAL OF BIOLOGICAL CHEMISTRY
Vol. 280, No. 21, Issue of May 27, pp. 20558–20564, 2005
Printed in U.S.A.

The Solution Structure of the FATC Domain of the Protein Kinase Target of Rapamycin Suggests a Role for Redox-dependent Structural and Cellular Stability*

Received for publication, January 31, 2005, and in revised form, March 10, 2005
Published, JBC Papers in Press, March 16, 2005, DOI 10.1074/jbc.M501116200

Sonja A. Dames‡§, José M. Mulet¶‖, Klara Rathgeb-Szabo‡, Michael N. Hall¶, and Stephan Grzesiek‡

From the Departments of ‡Structural Biology and ¶Biochemistry, Biozentrum, University of Basel, Klingelbergstrasse 70, 4056 Basel, Switzerland

The target of rapamycin (TOR) is a highly conserved Ser/Thr kinase that plays a central role in the control of cellular growth. TOR has a characteristic multidomain structure. Only the kinase domain has catalytic function; the other domains are assumed to mediate interactions with TOR substrates and regulators. Except for the rapamycin-binding domain, there are no high-resolution structural data available for TOR. Here, we present a structural, biophysical, and mutagenesis study of the extremely conserved COOH-terminal FATC domain. The importance of this domain for TOR function has been highlighted in several publications. We show that the FATC domain, in its oxidized form, exhibits a novel structural motif consisting of an α-helix and a COOH-terminal disulfide-bonded loop between two completely conserved cysteine residues. Upon reduction, the flexibility of the loop region increases dramatically. The structural data, the redox potential of the disulfide bridge, and the biochemical data of a cysteine to serine mutant indicate that the intracellular redox potential can affect the cellular amount of the TOR protein via the FATC domain. Because the amount of TOR mRNA is not changed, the redox state of the FATC disulfide bond is probably influencing the degradation of TOR.

Regulation of cellular growth is a prerequisite for cells, organs, and organisms to achieve a characteristic size. The target of rapamycin (TOR,[1] also known as FRAP, RAFT, RAPT, or SEPT) is a highly conserved 280-kDa Ser/Thr kinase that has been shown to play a central role in the control of cell growth in organisms ranging from yeast to human (1, 2). TOR proteins consist of several functional domains (see Fig. 1*a*) (3). The amino-terminal ~1200 residues consist of stretches of HEAT (huntingtin, elongation factor 3, regulatory subunit A of PP2A, TOR1) repeats, which typically mediate protein-protein interactions. Recently, it was also suggested that the ~550-amino acid-long FAT (FRAP, ATM, TTRAP) domain that follows the HEAT repeats is composed of HEAT repeat-like α-helical structures and could also serve as a protein interaction platform (4). The known interactions of TOR with other proteins have been reviewed recently (1, 2). The FKBP12-rapamycin binding site is flanked by the FAT domain and the catalytic kinase domain. Binding of the FKBP12·rapamycin complex to the FKBP12-rapamycin-binding domain specifically inhibits TOR (5). The catalytic kinase domain is highly homologous to that of phosphatidylinositol 3- and 4-kinases. Thus, TOR and its relatives have been termed phosphatidylinositol kinase-related kinases. TOR has been shown to fulfill its functions by directly phosphorylating serine and threonine residues of target proteins and by regulating protein phosphatases (1, 2). The carboxyl-terminal ~33 residues of TOR form the FATC domain. In all phosphatidylinositol kinase-related kinases, the FATC domain always occurs in tandem with the FAT domain (6). Previous studies have shown that the FATC domain is indispensable for TOR function *in vivo* and *in vitro* (7, 8).

Here, we report the solution structure of y1fatc, the FATC domain of yeast TOR1 (residues 2438–2470), which showed a new structural motif consisting of an α-helix and a disulfide-bonded loop. Reduction of the disulfide bond resulted in strong conformational changes and increased flexibility of the loop region. The structural data, together with the determined intermediate range redox potential (−0.23 V) and the biochemical characterization of a Cys to Ser mutant of the full-length protein, suggest that the cellular stability of TOR toward degradation and possibly its function can be redox-regulated.

EXPERIMENTAL PROCEDURES

Protein Expression—Constructs of the yeast TOR1 FATC (y1fatc) domain were designed based on sequence conservation. Residues 2438–2470 were cloned into GEV2 (9) using the BamHI and XhoI sites and overexpressed in *Escherichia coli* Rosetta (DE3) (Novagen) in M9 minimal medium. About 40% of the IgG-y1fatc fusion protein was in the soluble fraction obtained after sonication of the cells in 50 mM Tris-HCl, 2 mM EDTA, 2 mM benzamidine, pH 7.5. The remaining 60% of the protein was extracted from inclusion bodies. Inclusion bodies were washed with 20 mM Tris-HCl, 1 M urea, pH 7.5, and extracted using 50 mM Tris-HCl, 6 M guanidinium hydrochloride, pH 7.5, with agitation for 1 h at 4 °C. The extract was dialyzed to TST buffer (50 mM Tris buffer, pH 7.6, 150 mM NaCl, 0.05% Tween 20; equilibration buffer for the

* This work was supported in part by the Canton of Basel and Swiss National Science Foundation Grant 31-61 757.00 (to S. G. and M. N. H.). The costs of publication of this article were defrayed in part by the payment of page charges. This article must therefore be hereby marked "*advertisement*" in accordance with 18 U.S.C. Section 1734 solely to indicate this fact.

The atomic coordinates and structure factors (code 1W1N) have been deposited in the Protein Data Bank, Research Collaboratory for Structural Bioinformatics, Rutgers University, New Brunswick, NJ (http://www.rcsb.org/).

Chemical shift assignments have been deposited in the BioMagResBank under accession number 6228.

§ Supported by a postdoctoral fellowship from the Treubel Fonds (Basel, Switzerland). To whom correspondence should be addressed. Tel.: 41-61-2672107; Fax: 41-61-2672109; E-mail: sonja.dames@unibas.ch.

‖ Supported by a postdoctoral fellowship from the "Ministerio Español de Educación, Cultura y Deporte" and the European ACE Network.

[1] The abbreviations used are: TOR, target of rapamycin; mTOR, mammalian TOR; NOE, nuclear Overhauser effect; NOESY, NOE spectroscopy; FKBP12, peptidyl-prolyl isomerase FK506-binding protein of 12 kDa; IPAP-HSQC, in phase/antiphase-heteronuclear single quantum correlation; ROESY, rotational nuclear Overhauser effect spectroscopy; SED, spin echo difference; TOCSY, total correlation spectroscopy.

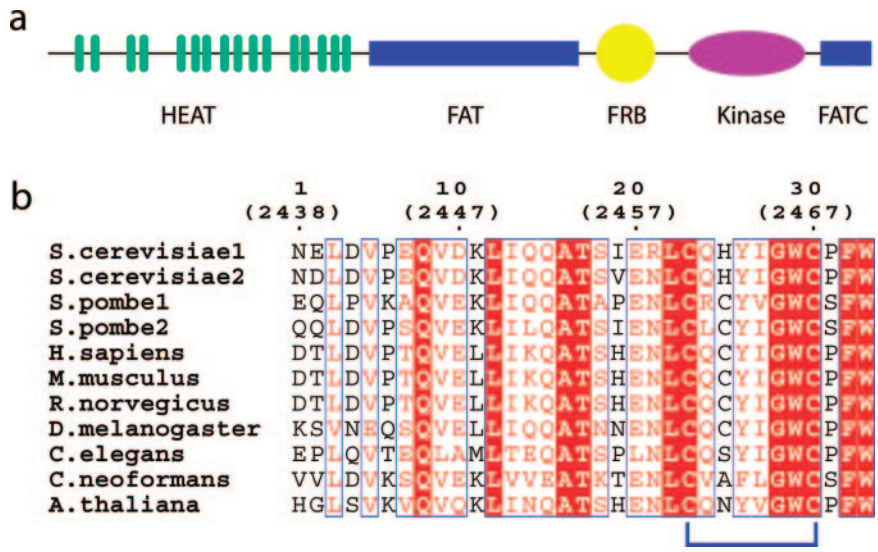

FIG. 1. The domain structure of the target of rapamycin protein is schematically depicted in *a*. *FRB*, FKBP12-rapamycin binding. An alignment of the amino acid sequences of the carboxyl-terminal FATC domain from TOR proteins from different organisms is given in *b*. The *numbering* in *parentheses* corresponds to yeast TOR1 (*top line*). Note the two conserved cysteines connected by a *blue line*. The sequence alignment was generated using the program ESPript (51).

IgG-Sepharose, see below). IgG-y1fatc fusion protein was extracted from the cleared lysate and from the dialyzed inclusion body extract using an IgG-Sepharose 6 fast flow column (Amersham Biosciences) as described in the manufacturer's manual. The purified fusion protein was lyophilized, resuspended in 50 mM Tris, 100 mM NaCl, pH 8, and desalted using a PD-10 column (Amersham Biosciences). The protein was eluted with 50 mM Tris-HCl, 100 mM NaCl, pH 8, and, after the addition of 2 mM $CaCl_2$, digested with Factor Xa (Amersham Biosciences) overnight. After digestion, the fusion partner was removed by reversed-phase high pressure liquid chromatography in an acetonitrile/trifluoroacetic acid buffer system, and fractions containing pure y1fatc were lyophilized. Electrospray mass spectrometry confirmed that y1fatc had the correct molecular weight. Analytical ultracentrifugation experiments of air oxidized y1fatc in 50 mM Tris, pH 7, showed that y1fatc was monomeric.

NMR Sample Preparation—Lyophilized ^{15}N- or $^{15}N,^{13}C$-labeled y1fatc was dissolved in 10 mM Tris, pH 8 (in 95% H_2O/5% D_2O or in 100% D_2O), and the pH was adjusted to 6. Reduced samples were obtained by adding 20 mM Tris(2-carboxylethyl)phosphine-HCl. The sample for measuring residual dipolar couplings contained about 25 mg/ml PF1 phages (ASLA Biotech). The protein concentration was always ~0.5 mM.

NMR Spectroscopy—NMR spectra were acquired at 298 K on Bruker DRX600 and 800 spectrometers. The data were processed with NMRPipe (10) and analyzed using NMRView (11). Assignments for ^{13}C, ^{15}N, and ^{1}H nuclei were based on three-dimensional CBCANH, CBCA(CO)NH, HBHA(CBCACO)NH, CCONH-TOCSY (12) and HCCH-TOCSY, and HNCO spectra. Stereospecific assignments and dihedral angle information were derived from 3D-HACAHB-COSY, 3D-^{15}N-ROESY, 3D-HNHA, and ^{13}CO-{$^{13}C\gamma$}-SED- and ^{15}N-{$^{13}C\gamma$}-SED-^{15}N-^{1}H-HSQC spectra. Distance restraints were obtained from ^{15}N- and ^{13}C-edited NOESY spectra. Information about the backbone dynamics was derived from the measurement of ^{15}N relaxation experiments including T_1 (spin-lattice or longitudinal relaxation rate), T_2 (spin-spin or transverse relaxation rate), and (^{1}H)-^{15}N NOE. If not explicitly mentioned elsewhere, references for all experiments are given in Ref. 13 and references therein. ^{15}N-^{1}H residual dipolar couplings were obtained from the analysis of ^{15}N-^{1}H IPAP-HSQC data (14) acquired on the sample containing PF1 phages. The maximal $^{1}D_{N\text{-}H}$ was −17.4 Hz.

Structure Calculation—All structure calculations were performed with XPLOR-NIH (15) using torsion angle molecular dynamics. Distance restraints were generated in NMRView and classified according to NOE cross-peak intensities. Upper bounds were 2.8, 3.4 (3.5 for ^{15}N-bound protons), 4.5, and 5.5 Å. The lower bound was always 1.8 Å. For all NOE restraints, r^{-6} sum averaging was used. Backbone dihedral angle restraints for ϕ were derived based on $^{3}J_{HNH\alpha}$ and the chemical shift index (16). Stereospecific assignments were obtained for 14 β-methylene proton pairs. Based on $^{3}J_{H\alpha H\beta 2/3}$ coupling constants and NOE/ROE data, side chain $\chi 1$ angles were restrained to one of the staggered conformations (60°, 180°, −60°) ± 30°. N-H residual dipolar couplings were included using the SANI statement and an error bound of 0.2 Hz. The distance between the Cα atoms of the disulfide bond-forming cysteines was restrained to be within 4.2–7.0 Å and the dihedral angle around the disulfide bond to be 0° ± 105°, because the dihedral angle $\chi 3$ is always 95° or −95° ± 10° (17).

Determination of the Redox Potential—The redox potential of y1fatc was determined by following the protein fluorescence at 350 nm for different ratios of reduced and oxidized glutathione ($[GSH]^2/[GSSG]$) and analyzing the data as described previously (18). Samples contained 1.1 μM y1fatc in 10 mM Tris-HCl, pH 7, 0.1 mM EDTA, 0.1 mM GSSG, and concentrations of GSH ranging from 10 μM to 90 mM. All buffers were degassed and flushed with argon. The concentration of reduced glutathione in the buffer was verified with an Ellman assay (19). All samples were prepared under nitrogen atmosphere. All measurements were performed at 25 °C (298 K) on an Aminco Bowman series 2 luminescence spectrometer using 1 × 1-cm quartz cuvettes (right angle arrangement), an excitation wavelength of 280 nm, and a bandwidth of 4 nm. The bandwidth for detection was 8 nm.

Mutagenesis Studies—Plasmid pJM244 ($pTOR2^{C\rightarrow S}$) was constructed by PCR amplification of a 1300-bp fragment of the COOH-terminal region of yeast TOR2 using the primers TOR2D (5′-GGT AAA CAG TTG CCA CAA TTA CAA TTA CAA ACT CTT GAA CTA CAA CAT GTG TCG CC) and TOR2Rmut (5′-GAA CTC GAG TAC AAC TAA GTG ATT TTC AAT ACA TTA AAA CTA CCA GAA TGG AGA CC) containing an artificial XhoI restriction site and a single base change (underlined) compared with the TOR2 wild-type sequence resulting in the C2470S mutation. The resulting PCR fragment was digested with SpeI and XhoI and used to substitute the SpeI-XhoI fragment of plasmid p206 (20), a yeast centromeric plasmid containing an NH_2-terminal hemagglutinin epitope-tagged TOR2 expressed under the control of its own promoter. Plasmid pJM232 (pTOR2) was constructed in a similar way, but with primer TOR2Rnat as TOR2Rmut and with a C instead of the underlined G, to amplify the wild-type sequence. As a control, the same centromeric plasmid without the TOR2 sequence (pRS314 = pVector) was used. No additional mutations were introduced in plasmids pJM232 and pJM244 as confirmed by sequencing of the SpeI-XhoI fragment. These plasmids were used to transform the *Saccharomyces cerevisiae* strains SH121 and SH221 (21). Yeast strains were grown in rich medium (yeast extract/peptone/dextrose) or synthetic minimal medium complemented with the appropriate nutrients for plasmid maintenance as described previously (22). Paromomycin and rapamycin were added at the indicated concentration from a concentrated stock to autoclaved yeast extract/peptone/dextrose with 2% agar prior to gelation. Spot tests of yeast growth were performed as described previously (23), but plates were incubated at a restrictive temperature (37 °C) for the thermosensitive allele of TOR2. Immunoprecipitation assays were performed as described previously (24).

RESULTS

The FATC Structure—The FATC domain of the family of TOR kinases is highly conserved. Fig. 1*b* shows an alignment of the carboxyl-terminal 33 residues of TOR proteins from different species. One-third of the residues are completely conserved, including two cysteines in an i to i + 7 spacing. To elucidate the role of the two cysteines for the structure of the FATC domain, we first acquired ^{15}N-HSQC spectra of oxidized and reduced

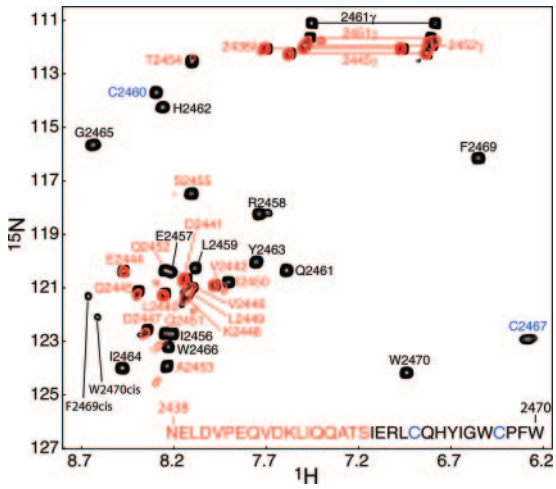

FIG. 2. **Two-dimensional ^{1}H-^{15}N HSQC spectrum of oxidized (*black peaks*) and reduced (*red peaks*) y1fatc.** The amino acid sequence of y1fatc is shown at the *bottom*. Reduction of the intramolecular disulfide bond between Cys^{2460} and Cys^{2467} increases the flexibility of the COOH-terminal half (depicted in *black letters* in the sequence). This increased flexibility broadens the resonances of the respective residues in the reduced form beyond detection.

y1fatc (Fig. 2). Oxidized y1fatc shows a spectrum characteristic for a folded protein with well dispersed amide proton nitrogen cross-peaks for the majority of residues. In the spectrum of the reduced form, resonances for the carboxyl-terminal 15 residues (2456–2470) were broadened beyond detection, indicating increased conformational flexibility because of the reduction of the disulfide bond in this region. To understand the molecular basis of the differences between the oxidized and the reduced forms, we have determined the structure of the oxidized form using standard NMR techniques.

The NMR structure of oxidized y1fatc is shown in Fig. 3, and structural statistics are given in Table I. The structure consists of a long, NH_2-terminal α-helix extending from residue Glu^{2444} to the first cysteine, Cys^{2460} (Fig. 3, *a* and *b*), and a COOH-terminal disulfide-bonded loop from Cys^{2460} to Cys^{2467} that folds the protein chain back onto itself. This chain reversal is facilitated by the completely conserved glycine at position 2465. Contacts within the loop are dominated by interactions involving aromatic side chains (Fig. 3*d*). Pro^{2468} makes hydrophobic as well as C-H···π interactions with the aromatic rings of Tyr^{2463}, Trp^{2466}, and Phe^{2469}. The C-H···π interactions are very similar to hydrogen bonds and depend on the orientation and distance of the planes of the involved pyrrolidine and aromatic rings (25). In y1fatc, many of the pyrrolidine ring protons of Pro^{2468} have distances of <4.5 Å to the aromatic carbons of Trp^{2466} and Phe^{2469} and orientations of their ring planes that are commonly found in such C-H···π interactions. Additional hydrophobic contacts involving aromatic and aliphatic side chains occur between the conserved carboxyl-terminal residues Phe^{2469} and Trp^{2470}, Leu^{2459} and Ile^{2456}, as well as between Trp^{2466}, Typ^{2463}, and Ile^{2464}. The side chains of Ile^{2456} and Leu^{2459} make further contacts to the methyl groups of Ala^{2453} and Thr^{2454}, respectively.

From a comparison of the ^{15}N-HSQC (Fig. 2) and circular dichroism (not shown) spectra of oxidized and reduced y1fatc, it can be deduced that part of the α-helix is also populated in the reduced form. The ^{1}H-^{15}N cross-peaks for the α-helical residues Glu^{2444} to Leu^{2449} do not shift significantly (Fig. 2), indicating that their chemical and structural environment is maintained. In contrast, the COOH-terminal region from Ile^{2456} to Trp^{2470} becomes clearly more flexible upon reduction of the Cys^{2460}–Cys^{2467} disulfide bridge.

The absence of NOEs for the first five NH_2-terminal residues preceding Pro^{2443} indicates a random coil conformation for this part of the sequence. Indeed, the ^{15}N relaxation data (Fig. 4) give evidence of large amplitude backbone motions on the subnanosecond time scale from V2442 onward to the NH_2 terminus because of a strong increase in the T_2 and T_1 relaxation times and a strong decrease of the (^{1}H)-^{15}N NOEs. T_1 values for the helical and loop part are more uniform, with an average of 0.57 ± 0.08 s, which is close to values expected for an isotropically tumbling molecule of the size of y1fatc (4 kDa) at 25 °C. In contrast, T_2 values (average = 0.10 ± 0.04 s) within this structured part are much smaller (~0.4 s) than expected for a rigid molecule of this size and indicate the presence of considerable line broadening because of chemical exchange on the microsecond time scale. Note also that the asymmetry of the helical molecule contributes to a certain extent to the shortening of the amide ^{15}N T_2 values. However, the effect of even very pronounced asymmetry of the diffusion tensor would be too small to account for the observed shortening of t_2. A more extended analysis using the program TENSOR (26) and an isotropic model as a first approximation for the rotational diffusion of y1fatc showed that the chemical exchange contributions (R_{ex}) increase strongly from the beginning to the end of the structured part (Fig. 4, *bottom panel*). The subnanosecond order parameter S^2 also increases from values around 0.3 at the NH_2 terminus to values around 0.8 at the COOH terminus (Fig. 4, *fourth panel*). Thus on the subnanosecond time scale, there are large amplitude motions at the NH_2 terminus but only small amplitude motions at the COOH-terminal end of the structure. In contrast, micro- to millisecond time scale motions are stronger in the COOH-terminal half. Therefore, albeit folded, the helix and loop parts of the FATC structure are partly flexible, with the time scale of motions becoming longer toward the COOH terminus. This observation is not surprising because the FATC domain is stabilized by only a few tertiary contacts at the COOH-terminal end that are mediated by the disulfide bridge.

The $^{13}C^{\alpha}$ and $^{1}H^{\alpha}$ resonances of Cys^{2467} are not visible in the NMR spectra of y1fatc, and its side chain and the one following residue Pro^{2468} show only few and broad NOE contacts. Presumably, this is because of additional conformational exchange from disulfide bond crankshaft motions like the ones that have been characterized in bovine pancreatic trypsin inhibitor (27). Indeed, in the structure calculations, the left-hand conformation (17) of the disulfide bond is only slightly more favored (13 of the 20 best structures) than the right-hand conformation.

A second minor set of resonances was observed for the backbone amides of residues Phe^{2469} and Trp^{2470} (Fig. 2) and for the Pro^{2468} Cδ/Hδ nuclei in the ^{13}C-HSQC spectrum. These resonances indicate the presence of a minor cis-form of Pro^{2468} in addition to the predominant trans-form. As judged from the spectral intensities, this cis-form is populated to 15–20%. Very similar structures for the rest of FATC were obtained when Pro^{2468} was constrained to the cis- instead of the trans-conformation (data not shown).

Determination of the Redox Potential—Because both tryptophans of y1fatc are in the vicinity of the disulfide bond-forming cysteines (Fig. 3*d*), the redox state-dependent fluorescence at 350 nm was used to determine the redox potential (18) of the Cys^{2460}–Cys^{2467} disulfide bond of y1fatc. For y1fatc equilibrated in buffers containing different ratios of oxidized and reduced glutathione, we detected a two-state transition curve (Fig. 5*a*) that corresponds to an equilibrium constant (K_{eq}) of 0.45 M. Using the Nernst equation $E'_{0\ y1fatc} = E'_{0\ GSH/GSSG} - (RT/2F) \ln K_{eq}$, with $E'_{0\ GSH/GSSG} = -0.24$ V, this results in a redox potential of −0.23 V for y1fatc. Apparently, this value is

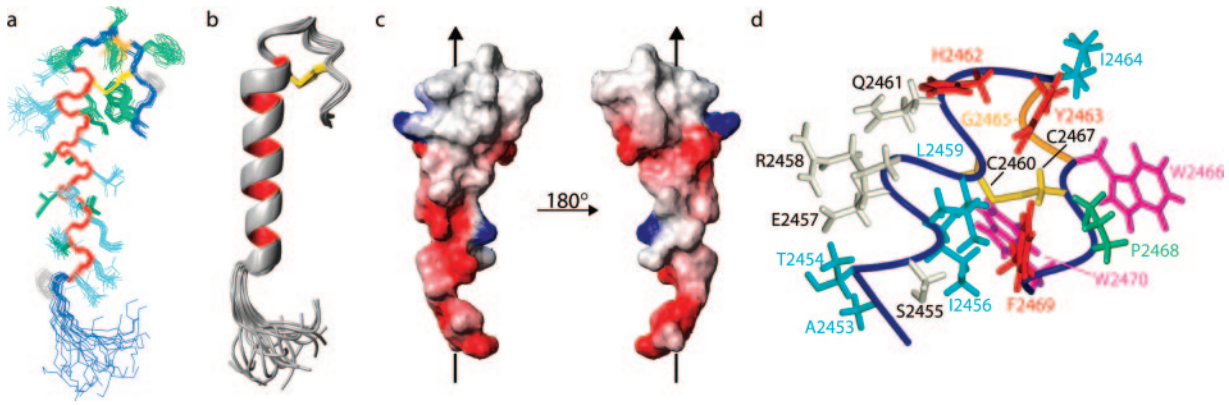

FIG. 3. **NMR structures of y1fatc (with Pro^{2468} in the major trans-conformation).** *a*, view of the 20 best structures of y1fatc after a least square alignment of the backbone atoms of residues 2443–2470. The backbone of the α-helix is *red*. The disulfide bond between cysteines 2460 and 2467 is *yellow*, and the conserved glycine (Gly^{2465}) is *orange*. Hydrophobic and aromatic side chains are *light green* in the picture foreground and *dark green* in the picture background, and polar or neutral amino acids side chains are *light blue*. *b*, ribbon representation of the 20 superposed structures from *a*. *c*, surface representation of the lowest energy structure from *a*. The surface is colored according to the charge distribution (*red*, negative; *blue*, positive). *d*, detailed view of the disulfide-bonded loop. All structure pictures were made with the programs MolMol (52) and POV-Ray.

TABLE I
Statistics for the final 20 of 200 calculated y1fatc structures (trans-Pro^{2468})

Experimental restraints	
Distance restraints	All (assigned + ambiguous)
Total	824 (727 + 97)
Intraresidue	399 (390 + 9)
Sequential + medium	389 (315 + 74)
Long range (|i-j| > 4)	36 (22 + 14)
ϕ angle restraints	26
χ_1 angle restraints	20
$^1D_{N-H}$ residual dipolar coupling restraints	29
Structural statistics[a]	
r.m.s.[b] deviations from experimental restraints	
Distance (Å)	0.0161 ± 0.0016
Dihedral angle (°)	0.347 ± 0.177
Residual dipolar coupling (Hz)	0.144 ± 0.024
r.m.s.[b] deviations from idealized geometry	
Bonds	0.0038 ± 0.0001
Angles	0.496 ± 0.017
Improper	0.365 ± 0.019
Lennard Jones energy (kcal mol^{-1})	−95 ± 5
Procheck[c] statistics (%)	
Residues in most favored regions	82.0
Residues in additional allowed regions	18.0
Residues in generously allowed regions	0
Residues in disallowed regions	0
Average r.m.s. deviation[b] to mean structure (Å)	
Residues 6–33 (backbone/heavy)	0.39/0.88
α-Helical = 7–23 (backbone/heavy)	0.22/0.83

[a] None of the structures had distance restraints violations >0.3 Å, dihedral angle violations >5°, or residual dipolar coupling violations >1 Hz.
[b] root mean square.
[c] Ref. 55.

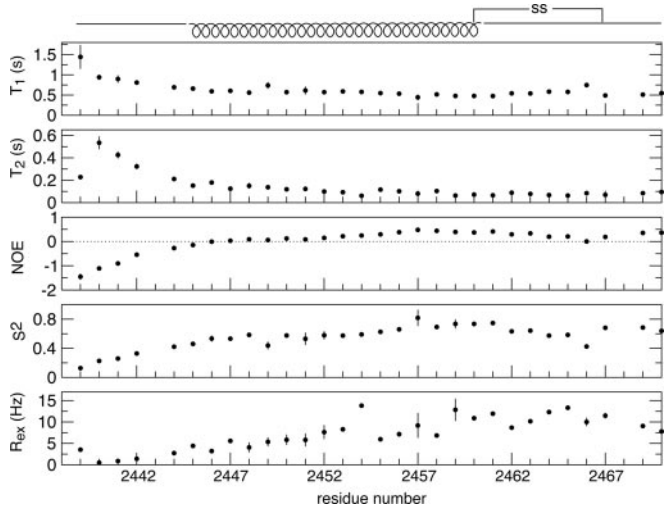

FIG. 4. **Backbone dynamics of y1fatc.** ^{15}N-T1 (*top panel*), T2 (*second panel*), and NOE (*third panel*) values and uncertainties were determined for the oxidized form of this 33-residue protein. Secondary structure elements and the location of the disulfide bond (*SS*) are indicated at the *top*. A model-free analysis (53, 54) of the ^{15}N relaxation data was performed using the program TENSOR2 (26). The analysis was based on an isotropic tumbling model with a rotational correlation time of 1.9 ns. The Lipari-Szabo model free order parameter S^2 and the contribution of chemical exchange R_{ex} to the observed transverse relaxation rate $1/T_2$ are displayed in the *bottom two panels*.

very close to the one for glutathione. Other cellular components (Fig. 5*b*) are more reducing or more oxidizing than y1fatc, such as thioredoxin (−0.27 V) or cytochrome *c* (0.22 mV), respectively.

Mutagenesis Studies—In yeast, two highly homologous TOR proteins have been identified. TOR1 is only found as part of TOR·C1 (complex 1), a multiprotein complex that regulates cell growth in a rapamycin-sensitive manner. In contrast, TOR2 can be found as part of TOR·C1 but additionally can participate in a second protein complex called TOR·C2. The known function of the complex TOR·C2 is to regulate the polarization of the actin cytoskeleton in a rapamycin-insensitive manner (24). To study the influence of the FATC disulfide bonds on both complexes, mutagenesis studies were carried out on the TOR2 protein.

In detail, the second of the disulfide bond-forming cysteines in TOR2 (Cys^{2470} = Cys^{2467} in TOR1) was changed to serine (C2470S). To investigate the effect of this TOR2 mutation on the function of the rapamycin-insensitive complex TOR·C2, a plasmid containing the C2470S mutation (pTOR2$^{C\rightarrow S}$) was introduced into the yeast strain SH121 (21) that carries a thermosensitive allele of *TOR2*. The pTOR2$^{C\rightarrow S}$ plasmid was able to complement the thermosensitive phenotype under restrictive temperature conditions (37 °C), where expression of wild-type TOR2 protein is suppressed (data not shown). Experiments with an isogenic wild-type plasmid (pTOR2) yielded

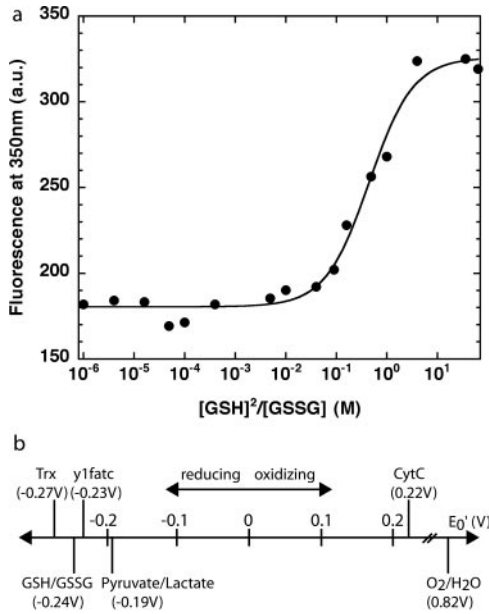

FIG. 5. **Determination of the redox potential of y1fatc.** The shown transition curve (*a*) was obtained by monitoring the fluorescence at 350 nm of samples containing 1.1 μM y1fatc, 0.1 mM oxidized glutathione, and varying concentrations of reduced glutathione (10 μM–90 mM). The experimental data were analyzed as described under "Experimental Procedures." *b*, scale of the redox potentials of some cellular components. Redox pairs to the *left* of y1fatc are more reducing, and those to the *right* of y1fatc are more oxidizing.

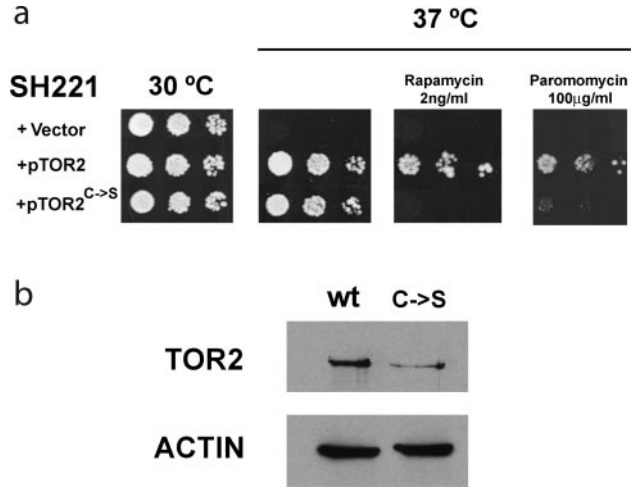

FIG. 6. **The cysteine to serine mutation in yeast TOR2 (C2470S) induces rapamycin and paromomycin hypersensitivity.** These phenotypes correlate with less TOR2 protein. *a*, at a restrictive temperature (37 °C), pTOR2$^{C\rightarrow S}$ is unable to grow in the presence of rapamycin or paromomycin. Precultures of the indicated strains were grown in selective synthetic minimal media until saturation. Water dilutions of each strain (1/10, 1/100, and 1/1000) were spotted on yeast extract/peptone/dextrose medium containing the indicated concentration of rapamycin or paromomycin, and growth was recorded after 4 days. Identical results were obtained from at least six independent colonies of each strain in two separate experiments. *b*, TOR2$^{C\rightarrow S}$ protein is less abundant than TOR2 protein. Cells expressing hemagglutinin-TOR2 (wild type (*wt*)) and hemagglutinin-TOR2$^{C\rightarrow S}$ (*C→S*) were grown (at 37 °C) and harvested, and the protein was extracted in the same way. The protein concentration was determined by a Bradford assay. Both cell lysates were subjected to immunoprecipitation with anti-hemagglutinin, and the resulting precipitates were resolved by SDS-PAGE and Western blotted to detect TOR2. As a control, actin was immunoprecipitated in parallel (*bottom panel*).

identical results. Thus, the function of complex TOR·C2 is not affected by the C2470S mutation.

To investigate the effect of the C2470S mutation on the function of the rapamycin-sensitive complex TOR·C1, the pTOR2$^{C\rightarrow S}$ plasmid was introduced into the yeast strain SH221 that is deleted in *TOR1* and carries a thermosensitive allele of *TOR2* (21). Switching from the permissive (30 °C) to the restrictive temperature (37 °C) under normal or stressful conditions, including oxidative or osmotic stress, did not lead to a growth defect (data not shown). However, at the restrictive temperature, the strain carrying plasmid pTOR2$^{C\rightarrow S}$ was unable to grow on medium containing sublethal concentrations of paromomycin, a protein synthesis inhibitor, or of rapamycin, a TOR-C1-specific inhibitor (Fig. 6*a*). In contrast, controls at the permissive temperature or on the same strain transformed with the plasmid pTOR2 showed normal growth (Fig. 6*a*). Thus the C2470S mutation affects the activity of the rapamycin-sensitive complex TOR·C1 in the presence of paromomycin or rapamycin.

This effect on the activity could be caused by a structural change within the complex or by a general destabilization of TOR2 that leads to smaller cellular concentrations. To investigate this effect further, we performed an immunoprecipitation of TOR2 extracted from yeast cells that were grown identically at the restrictive temperature (37 °C) and that were expressing either wild-type or mutated TOR2. The amount of C2470S TOR2 was ~3-fold less than that of wild-type TOR2 (Fig. 6*b*). Thus, the C2470S mutation reduces the amount of TOR2 protein, which may explain the paromomycin- and rapamycin-hypersensitive phenotypes described above. To make sure that the mutation does not simply affect the amount of TOR2 on the mRNA level, we performed reverse transcription-PCR experiments (data not shown) using the same strains, genetic constructs, and growth conditions as for the immunoprecipitation. These experiments showed that the mutation does not change either the transcription or, presumably, the expression level of TOR2 (data not shown). We also performed immunofluorescence experiments on whole fixed cells to determine the cellular location of the mutant TOR2, but no changes in localization compared with wild-type TOR2 were detected (data not shown).

DISCUSSION

In the present study, we investigated the structure of the highly conserved yeast TOR1 FATC domain. In its oxidized form, FATC consists of an α-helix and a well structured disulfide-bonded loop between two completely conserved cysteines (Cys^{2460} and Cys^{2467}). The NH_2-terminal half of the helix and the loop region next to the COOH terminus are rather acidic (Fig. 3*c*), whereas the remaining part of the loop is more hydrophobic. Therefore, oxidized FATC could bind to a hydrophobic surface of complementary shape surrounded by polar residues. Reduction of the disulfide bond dramatically increases the flexibility within the COOH-terminal loop region and presumably the accessibility of several hydrophobic side chains in this region. Thus the reduction may alter the binding behavior of FATC to other parts of TOR or other cellular partners.

The redox potential of the Cys^{2460}–Cys^{2467} disulfide bridge was determined as −0.23 V. This value is very similar to the one for glutathione (Fig. 5*b*). In yeast, a C2470S TOR2 mutation had no significant effect on growth under normal or stressful conditions. However, cells carrying the TOR2 C2470S mutation were hypersensitive to rapamycin and paromomycin. This observation, together with the fact that TOR2 carrying the C2470S mutation is less abundant than wild-type TOR2, indicates that the cellular amount of TOR is affected by the redox state of the FATC domain. Because the level of TOR mRNA is not changed, the redox state of the FATC disulfide bond is probably influencing the degradation of TOR.

Commonly, the cytosol is considered to be a reducing envi-

ronment. Very few values of the redox potential in living cells have been reported. The determination of appropriate values is hampered because the intracellular redox potential may depend on the location, metabolic state, differentiation, and type of the cell. The redox potential for the overall intracellular environment of a mammalian cell line was determined to range from −0.221 to −0.236 V (28). Using a green fluorescent protein with an engineered disulfide bond (rxYFP), the redox potential of the cytosolic glutathione pool of wild-type yeast cells under normal growth conditions was determined to be −0.289 V but changed to −0.227 V upon mutation of genes involved in the regulation of the cytosolic glutathione pool (29). During the life cycle of mammalian cells, the cytosolic redox potential was found to range between ~−0.260 and −0.160 V (30). In proliferating mammalian cells, the redox potential is ~−0.24 V (28, 31, 32), whereas more oxidizing conditions are found in differentiating cells (~−0.2 V) (30) and at the onset of apoptosis (~−0.17 to −0.19 V) (31, 32). TOR has also been found in the nucleus (33). However, to our knowledge, no information is available on the redox potential within the nucleus.

Based on the reported cellular redox potentials, it is possible that TOR exists in both reduced and oxidized forms in the cellular environment. The ratio of oxidized to reduced TOR during the cellular life cycle could be altered through the action of typical cellular redox regulators (glutathione, thioredoxin, glutathione *S*-transferase, cytochrome *c*, reactive oxygen species, etc.), in which concentrations depend on metabolic activities in response to the availability of nutrients, the action of growth hormones, and the influence of stress (oxidative, UV, etc.). Furthermore, the local redox potential for the FATC disulfide bond may be modulated within the various TOR complexes.

Several examples exist of cytosolic and nuclear proteins that are regulated through the reversible oxidation of a cysteine side chain. The roles of redox-sensitive proteins involved in stress responses (34), regulation of cell death (35), and cancer proliferation (36) have been reviewed recently. Within the TOR signaling cascade, various redox-dependent proteins or processes have been reported. For example, the lipid phosphatase PTEN, a tumor suppressor, is redox-regulated. Mutations or loss of PTEN are associated with an increased activation of mTOR (37, 38). PTEN is inactivated through the reversible formation of a disulfide bond in its active site (39). Furthermore, it has been suggested that mTOR is involved in the regulation of hypoxia-inducible factor 1α (40–43) and that hypoxia can trigger hypophosphorylation of mTOR and some of its effectors in a hypoxia-inducible factor-independent manner (41). Obviously low oxygen pressure (hypoxia) should influence the redox potential within the cell. Additionally, it has been suggested that the UV response pathway induces the phosphorylation of p70 S6 kinase in an mTOR-dependent manner via the generation of reactive oxygen species (44). Finally, TOR can associate with the mitochondrial outer membrane (45), which could make it directly susceptible to (redox) signals from this organelle.

The effect of mutations within the mTOR FATC domain has been investigated in two studies (7, 8). Both show that deletion of the carboxyl-terminal tryptophan as well as small deletions (three or more residues) of the COOH terminus abolish mTOR autophosphorylation activity as well as mTOR-dependent phosphorylation of eukaryotic initiation factor 4E-binding protein and p70 S6 kinase. Thus, the COOH-terminal deletions abolished mTOR function. These findings indicate that the FATC domain interacts with other parts of TOR or other components of TOR complexes (24, 46–49) to activate kinase function. Notably, a C2546A mutation in the FATC domain of mTOR did not prevent mTOR from autophosphorylating or activating p70 S6 kinase (7). Nevertheless, from the autoradiogram presented, it can be concluded that the degree of p70 S6 kinase activation was lower for mutated than for wild-type mTOR. In agreement with these data, our C2470S yeast TOR2 mutant is also still active, but its cellular concentration is lowered.

In conclusion, we have presented the structure of the FATC domain of yeast TOR1. FATC forms a novel structural motif consisting of an α-helix and a COOH-terminal disulfide-bonded loop. Upon reduction of this disulfide bond, the flexibility of FATC increases dramatically. Considering that several redox-dependent processes can be connected to the TOR signaling cascade, it seems attractive to propose that the function of TOR can be redox-regulated via the highly conserved FATC disulfide bond. Our data indicate that the redox potential of the disulfide bond is in an intermediate range and that the cellular amount of TOR is affected by the C2470S mutation. An analogous redox-regulatory mechanism for the cellular stability of a protein has been suggested for the phosphatase Cdc25C, which is involved in the regulation of cell cycle progression (50). Future biochemical and structural experiments will be required to shed light on the influence of changes in the cytosolic redox potential on the FATC domain and its interactions with other TOR domains or components of TOR complexes.

Acknowledgments—We thank Prof. Rudi Glockshuber for useful suggestions and comments for the determination of the redox potential, the group of Prof. Thomas Kiefhaber for help with the use of their fluorescence spectrometer, Marco Rogowski for running the fermenter, Ariel Lustig for the ultracentrifugation experiments, Andrea Löschmann-Hage for help with the cloning, the group of Dr. Paul Jenö for the mass spectrometry data, and Drs. Florence Cordier and Sebastian Meier for help with the NMR experiments.

REFERENCES

1. Jacinto, E., and Hall, M. N. (2003) *Nat. Rev.* **4,** 117–126
2. Harris, T. E., and Lawrence, J. C., Jr. (2003) *Sci. STKE* **2003,** re15
3. Schmelzle, T., and Hall, M. N. (2000) *Cell* **103,** 253–262
4. Perry, J., and Kleckner, N. (2003) *Cell* **112,** 151–155
5. Zheng, X. F., Florentino, D., Chen, J., Crabtree, G. R., and Schreiber, S. L. (1995) *Cell* **82,** 121–130
6. Bosotti, R., Isacchi, A., and Sonnhammer, E. L. (2000) *Trends Biochem. Sci.* **25,** 225–227
7. Takahashi, T., Hara, K., Inoue, H., Kawa, Y., Tokunaga, C., Hidayat, S., Yoshino, K., Kuroda, Y., and Yonezawa, K. (2000) *Genes Cells* **5,** 765–775
8. Peterson, R. T., Beal, P. A., Comb, M. J., and Schreiber, S. L. (2000) *J. Biol. Chem.* **275,** 7416–7423
9. Huth, J. R., Bewley, C. A., Jackson, B. M., Hinnebusch, A. G., Clore, G. M., and Gronenborn, A. M. (1997) *Protein Sci.* **6,** 2359–2364
10. Delaglio, F., Grzesiek, S., Vuister, G. W., Zhu, G., Pfeifer, J., and Bax, A. (1995) *J. Biomol. NMR* **6,** 277–293
11. Johnson, B. R., and Blevins, R. A. (1994) *J. Biomol. NMR* **4,** 603–614
12. Grzesiek, S., Anglister, J., and Bax, A. (1993) *J. Magn. Reson.* **101,** 114–119
13. Grzesiek, S., Bax, A., Hu, J. S., Kaufman, J., Palmer, I., Stahl, S. J., Tjandra, N., and Wingfield, P. T. (1997) *Protein Sci.* **6,** 1248–1263
14. Ottiger, M., Delaglio, F., and Bax, A. (1998) *J. Magn. Reson.* **131,** 373–378
15. Schwieters, C. D., Kuszewski, J. J., Tjandra, N., and Marius Clore, G. (2003) *J. Magn. Reson.* **160,** 65–73
16. Wishart, D. S., and Sykes, B. D. (1994) *J. Biomol. NMR* **4,** 171–180
17. Richardson, J. S. (1981) *Adv. Protein Chem.* **34,** 167–339
18. Grauschopf, U., Fritz, A., and Glockshuber, R. (2003) *EMBO J.* **22,** 3503–3513
19. Creigthon, T. E. (1993) *Proteins*, 2nd Ed., pp. 157–158, W. H. Freeman and Co., New York
20. Jiang, Y., and Broach, J. R. (1999) *EMBO J.* **18,** 2782–2792
21. Helliwell, S. B., Howald, I., Barbet, N., and Hall, M. N. (1998) *Genetics* **148,** 99–112
22. Sherman, F. (1991) *Methods Enzymol.* **194,** 3–21
23. Mulet, J. M., Alejandro, S., Romero, C., and Serrano, R. (2004) *Yeast* **21,** 569–582
24. Loewith, R., Jacinto, E., Wullschleger, S., Lorberg, A., Crespo, J. L., Bonenfant, D., Oppliger, W., Jenoe, P., and Hall, M. N. (2002) *Mol. Cell* **10,** 457–468
25. Bhattacharyya, R., and Chakrabarti, P. (2003) *J. Mol. Biol.* **331,** 925–940
26. Dosset, P., Hus, J. C., Blackledge, M., and Marion, D. (2000) *J. Biomol. NMR* **16,** 23–28
27. Grey, M. J., Wang, C., and Palmer, A. G., III (2003) *J. Am. Chem. Soc.* **125,** 14324–14335
28. Hwang, C., Sinskey, A. J., and Lodish, H. F. (1992) *Science* **257,** 1496–1502
29. Ostergaard, H., Tachibana, C., and Winther, J. R. (2004) *J. Cell Biol.* **166,**

337–345
30. Kirlin, W. G., Cai, J., Thompson, S. A., Diaz, D., Kavanagh, T. J., and Jones, D. P. (1999) *Free Radic. Biol. Med.* **27,** 1208–1218
31. Cai, J., and Jones, D. P. (1998) *J. Biol. Chem.* **273,** 11401–11404
32. Cai, J., Wallace, D. C., Zhivotovsky, B., and Jones, D. P. (2000) *Free Radic. Biol. Med.* **29,** 334–342
33. Zhang, X., Shu, L., Hosoi, H., Murti, K. G., and Houghton, P. J. (2002) *J. Biol. Chem.* **277,** 28127–28134
34. Linke, K., and Jakob, U. (2003) *Antioxid. Redox Signal* **5,** 425–434
35. Fernandez-Checa, J. C. (2003) *Biochem. Biophys. Res. Commun.* **304,** 471–479
36. Loo, G. (2003) *J. Nutr. Biochem.* **14,** 64–73
37. Podsypanina, K., Lee, R. T., Politis, C., Hennessy, I., Crane, A., Puc, J., Neshat, M., Wang, H., Yang, L., Gibbons, J., Frost, P., Dreisbach, V., Blenis, J., Gaciong, Z., Fisher, P., Sawyers, C., Hedrick-Ellenson, L., and Parsons, R. (2001) *Proc. Natl. Acad. Sci. U. S. A.* **98,** 10320–10325
38. Neshat, M. S., Mellinghoff, I. K., Tran, C., Stiles, B., Thomas, G., Petersen, R., Frost, P., Gibbons, J. J., Wu, H., and Sawyers, C. L. (2001) *Proc. Natl. Acad. Sci. U. S. A.* **98,** 10314–10319
39. Leslie, N. R., Bennett, D., Lindsay, Y. E., Stewart, H., Gray, A., and Downes, C. P. (2003) *EMBO J.* **22,** 5501–5510
40. Hudson, C. C., Liu, M., Chiang, G. G., Otterness, D. M., Loomis, D. C., Kaper, F., Giaccia, A. J., and Abraham, R. T. (2002) *Mol. Cell. Biol.* **22,** 7004–7014
41. Arsham, A. M., Howell, J. J., and Simon, M. C. (2003) *J. Biol. Chem.* **278,** 29655–29660
42. Humar, R., Kiefer, F. N., Berns, H., Resink, T. J., and Battegay, E. J. (2002) *FASEB J.* **16,** 771–780
43. Treins, C., Giorgetti-Peraldi, S., Murdaca, J., Semenza, G. L., and Van Obberghen, E. (2002) *J. Biol. Chem.* **277,** 27975–27981
44. Huang, C., Li, J., Ke, Q., Leonard, S. S., Jiang, B. H., Zhong, X. S., Costa, M., Castranova, V., and Shi, X. (2002) *Cancer Res.* **62,** 5689–5697
45. Desai, B. N., Myers, B. R., and Schreiber, S. L. (2002) *Proc. Natl. Acad. Sci. U. S. A.* **99,** 4319–4324
46. Kim, D. H., Sarbassov, D. D., Ali, S. M., King, J. E., Latek, R. R., Erdjument-Bromage, H., Tempst, P., and Sabatini, D. M. (2002) *Cell* **110,** 163–175
47. Hara, K., Maruki, Y., Long, X., Yoshino, K., Oshiro, N., Hidayat, S., Tokunaga, C., Avruch, J., and Yonezawa, K. (2002) *Cell* **110,** 177–189
48. Wedaman, K. P., Reinke, A., Anderson, S., Yates, J., III, McCaffery, J. M., and Powers, T. (2003) *Mol. Biol. Cell* **14,** 1204–1220
49. Kunz, J., Schneider, U., Howald, I., Schmidt, A., and Hall, M. N. (2000) *J. Biol. Chem.* **275,** 37011–37020
50. Savitsky, P. A., and Finkel, T. (2002) *J. Biol. Chem.* **277,** 20535–20540
51. Gouet, P., Robert, X., and Courcelle, E. (2003) *Nucleic Acids Res.* **31,** 3320–3323
52. Koradi, R., Billeter, M., and Wuthrich, K. (1996) *J. Mol. Graph.* **14,** 51–55, 29–32
53. Lipari, G., and Szabo, A. (1982) *J. Am. Chem. Soc.* **104,** 4546–4559
54. Lipari, G., and Szabo, A. (1982) *J. Am. Chem. Soc.* **104,** 4559–4570
55. Laskowski, R. A., Rullmannn, J. A., MacArthur, M. W., Kaptein, R., and Thornton, J. M. (1996) *J. Biomol. NMR* **8,** 477–486

The Solution Structure of the FATC Domain of the Protein Kinase Target of Rapamycin Suggests a Role for Redox-dependent Structural and Cellular Stability

Sonja A. Dames, José M. Mulet, Klara Rathgeb-Szabo, Michael N. Hall and Stephan Grzesiek

J. Biol. Chem. 2005, 280:20558-20564.
doi: 10.1074/jbc.M501116200 originally published online March 16, 2005
